The Astrophysical Journal, 623:911–916, 2005 April 20

OBSERVATIONS OF DIFFUSE EXTREME-ULTRAVIOLET EMISSION WITH THE *COSMIC HOT INTERSTELLAR PLASMA SPECTROMETER* (*CHIPS*)

M. Hurwitz
Space Sciences Laboratory, University of California at Berkeley, 7 Gauss Way, Berkeley, CA 94720-7450;
markh@ssl.berkeley.edu

T. P. Sasseen
Department of Physics, University of California, Santa Barbara, CA 93106

and

M. M. Sirk
Space Sciences Laboratory, University of California at Berkeley, 7 Gauss Way, Berkeley, CA 94720-7450
Received 2004 March 30; accepted 2004 December 27

ABSTRACT

The *Cosmic Hot Interstellar Plasma Spectrometer* (*CHIPS*) was designed to study diffuse emission from hot gas in the local interstellar cavity in the wavelength range 90–265 Å. Between launch in 2003 January and early 2004, the instrument was operated in narrow-slit mode, achieving a peak spectral resolution of about 1.4 Å FWHM. Observations were carried out preferentially at high Galactic latitudes; weighted by observing time, the mean absolute value of the Galactic latitude for all narrow-slit observations combined is about 45°. The total integration time is about 13.2 Ms (74% day, 26% night). In the context of a standard collisional ionization equilibrium plasma model, the *CHIPS* data set tight constraints on the emission measure at temperatures between $10^{5.55}$ and $10^{6.4}$ K. At $10^{6.0}$ K, the 95% upper limit on the emission measure is about 0.0004 cm^{-6} pc for solar-abundance plasma with a foreground neutral hydrogen column of 2×10^{18} cm^{-2}. This constraint, derived primarily from limits on the extreme ultraviolet emission lines of highly ionized iron, is well below the range for the local hot bubble estimated previously from soft X-ray studies. If the pattern of elemental depletion in the hot gas follows that observed in much denser interstellar clouds, the gas-phase abundance of iron, relative to other heavy elements that contribute more to the soft X-ray emission, might be much lower than solar. However, to support the emission measures inferred previously from X-ray data would require depletions much higher than the moderate values reported previously for hot gas. Excluding the He II Lyman lines, which are known to be primarily terrestrial in origin, the brightest feature we find in the integrated spectrum is an Fe IX line at 171.1 Å. The sky-averaged flux of the feature is about 6 photons cm^{-2} s^{-1} sr^{-1}, a flux that exceeds the 1 σ shot noise significantly but is comparable to the systematic uncertainty. We find bright 171.1 Å emission (flux greater than 10 photons cm^{-2} s^{-1} sr^{-1} and S/N > 2) in about 10% of the observing time. However, these bright observations overwhelmingly select for daytime (96% of 1.3 Ms). Thus, a local rather than interstellar origin for much of the 171.1 Å emission seems likely.

Subject headings: Galaxy: abundances — ISM: bubbles — ISM: general — ISM: structure — solar neighborhood — ultraviolet: ISM

1. INTRODUCTION

Based on a number of methods of observation, the Sun is known to lie in a cavity of unusually low interstellar density. The cavity is believed to contain gas of temperature around 10^6 K, with a filling factor greater than 80%. Denser material at the cavity walls has been mapped in Na by Sfeir et al. (1999). These measurements show that the local cavity extends into the plane of the Galaxy about 100 pc, but much farther perpendicular to the plane, possibly connecting to the lower halo (Crawford et al. 2002).

Analysis of the spatial and spectral distribution of the diffuse X-ray background and H I shadowing reveal a relatively unabsorbed, "local" component with temperature about $10^{6.1}$ K, emission measure ranging from about 0.0018 to 0.0058 cm^{-6} pc, and a physical extent somewhat smaller than that of the boundary of the local cavity (Snowden et al. 1998; Kuntz & Snowden 2000; McCammon & Sanders 1990). The collisional ionization equilibrium (CIE) plasma emission codes employed in such modeling predict a cluster of emission lines of highly ionized iron (Fe VII–Fe XII) near 72 eV, with a combined strength of about 150–300 photons cm^{-2} s^{-1} sr^{-1} (hereafter "line units" or LU). For a solar-abundance plasma in CIE near 10^6 K, the flux in the iron lines comprises about 50% of the total radiated power. Thus, determining the strength of these lines observationally has implications for plasma lifetimes.

Within the cavity exist warm, partially ionized parcels of gas commonly called "clouds," in which the ionization fraction of helium is at or above that of hydrogen, despite helium's much higher ionization potential (Kimble et al. 1993). Fossil nonequilibrium ionization can, in principle, provide an explanation for this puzzle, but the simplest scenario, in which the clouds are recombining from a past impulsive event, is difficult to reconcile with the abundance of neutral argon in these clouds (Jenkins et al. 2000). For a solar-abundance plasma in CIE near 10^6 K, the EUV iron lines provide about 90% of the helium-ionizing photons (weighting by the photoionization cross section).

Thus, a picture has arisen in which nearby interstellar clouds are photoionized, with stellar sources providing the bulk of the hydrogen-ionizing photons, and the "local hot bubble" (the hot medium itself, and/or its interfaces with cooler gas) providing the bulk of the helium-ionizing photons (Vallerga & Welsh 1995).

Within this framework, several outstanding puzzles remain. Interaction of the solar wind with the Earth's exosphere (Freyberg 1998) and/or gas within the heliosphere (Lallement et al. 2004) may produce a substantial fraction of the observed soft X-ray background, reducing the need for a local, hot interstellar component. When the so-called long-term enhancements in X-ray data are properly treated, the contribution from Earth's exosphere can be limited to a small fraction of the observed signal (Cravens et al. 2001), but the remaining contributions are more difficult to constrain. The few existing spectra of the X-ray background reveal thermal line emission, but even an approximate fit to the data requires depleted abundances and a complex temperature structure (Sanders et al. 2001). Several observations, discussed below, have suggested that the energetically important iron line complex near 72 eV is weaker than expected, also potentially implicating abundance effects and/or nonequilibrium ionization (the nonequilibrium model of Breitschwerdt & Schmutzler [1994], for example, generally matches the broadband X-ray colors while producing virtually no EUV line emission). Thus, the key physical parameters, such as temperature(s), emission measure, elemental abundances, and ionization conditions in the local hot bubble, remain uncertain.

The *Cosmic Hot Interstellar Plasma Spectrometer* (*CHIPS*), NASA's first and to date only University-class Explorer, was designed to survey the sky for diffuse emission in the relatively unexplored band from about 90 to 265 Å. Of particular interest is the cluster of emission features of Fe VIII–Fe XII between about 168 and 195 Å. Their close wavelength spacing and common elemental origin make them an excellent thermometer. *CHIPS*'s primary performance goal was to resolve these features. Subject to this resolution requirement, and the constraints imposed by the limited resources of the mission, the instrument was designed to maximize sensitivity near 170 Å, and secondarily to include as wide a bandpass as feasible. In this paper, we discuss data obtained in the first year or so of the *CHIPS* mission and briefly describe the tests used to verify the performance of the spectrograph on orbit.

2. OBSERVATIONS AND DATA REDUCTION

CHIPS shares the orbit of *ICESat* (*Ice, Cloud, and land Elevation Satellite*), the primary payload on the launch vehicle. The orbit is approximately circular at 600 km and an inclination of 94°. With all slits open, the spectrograph field of view is roughly rectangular at 5° by 25°. The data presented in this work were collected in narrow-slit mode, with a peak resolution of about 1.4 Å FWHM.

We refer to a specific field on the sky (i.e., a certain boresight and instrument roll angle) as a target. The selection of targets is influenced by the demands of the spacecraft power and thermal budgets and the capabilities of the attitude-control system. Within these constraints, we have sought to achieve deep integrations on high Galactic latitude regions where, based on soft X-ray studies, the EUV emission was expected to be brightest, while also sampling low and moderate latitudes. Individual pointings are of ~20 minute duration, typical of observatories in low Earth orbit.

The *CHIPS* spectrograph has six independent grating channels dispersing diffuse emission across a common detector. Thin-film filters attenuate out-of-band and scattered light. A diffuse emission line spans the full available detector height, and most wavelengths land upon two distinct filters. The emission features of iron are covered by both an aluminum filter (the large aluminum panel) and a zirconium filter. Additional details regarding the science instrument and satellite are presented in Hurwitz et al. (2003), Janicik et al. (2003), Marckwordt et al. (2003), Sirk et al. (2003), and Sholl et al. (2003).

We apply several filters to the raw data in producing the reduced spectra. Data are excluded when the overall detector count rate exceeds 80 events s^{-1}, indicative of high charged-particle backgrounds. Data are also excluded when the detector high voltage is reduced (a normal, temporary response to transient high-background periods). A broad pulse-height filter is applied by the flight software. Approximately 40% of the telemetered events are then excluded by a pulse-height threshold in ground software, selectively reducing background, because the low-amplitude events are overwhelmingly triggered by charged particles rather than by photons.

The data analysis pipeline automatically splits the photon data from each target into daytime and nighttime spectra. We refer to each day or night spectrum as an "observation." Because of the observing constraints mentioned above, there is a strong correlation between a target's coordinates and its availability in the orbital day/night cycle. The calendar year (CY) 2003–2004 narrow-slit observing program resulted in 244 targets and 355 observations.

In Figure 1, we show the boresight locations, in Galactic coordinates, of the targets analyzed in this work. All narrow-slit data from CY 2003 and CY 2004 are included; each target is indicated by a plus sign. For targets in which either the day or night observation resulted in an unusually high EUV flux (discussed below), a larger diamond surrounds the plotting symbol. Weighted by observing time, the average absolute value of the Galactic latitude of the observed targets is about 45°.

Periodically pulsed "stimulation pins" outside the active field of view are used to register the event x,y coordinates to a common frame, thereby correcting for thermal drifts in the plate scale or zero points, and to determine the effective time of the observation. Distortion is corrected using a preflight pinhole grid map. Small regions of known detector "hot spots" are excluded, the event coordinates are rotated so that the new x-axis closely corresponds to the spectral dispersion direction, and the spectra in each filter half are summed over the active detector height.

To determine the continuum against which to search for emission lines, we use a very deep flight charged-particle spectrum, scaled to match the local counts in the spectrum under analysis. The deep charged-particle spectrum generally contains many more photon events per wavelength interval than does the spectrum under analysis, and thus contributes relatively little to the shot noise in the line flux. Differences in the technique by which the scale factor is determined (for example, heavy smoothing vs. fitting low-order polynomials) changes the measured flux by no more than 10%.

Because it was expected that backgrounds would be brighter than the photon signals of interest, we paid careful attention to systematic effects. To determine the absolute flatness of the detector response, we analyzed a preflight photon flat field that was histogrammed like the flight spectra. Compared to a smooth polynomial, the flat-field spectrum showed a pixel-to-pixel variance only slightly greater than expected for shot noise, where "pixel" refers to the width of the narrowest spectral features. The excess 1 σ variance above shot noise was about 0.3% of the total signal. Thus, in very deep spectra in which shot noise is negligible, excursions greater than 0.3% compared to a locally smooth continuum are "real" at the 1 σ level even without application of any flat-field correction.

To explore the smoothness of the detector backgrounds in flight, we applied an analysis similar to the one described above

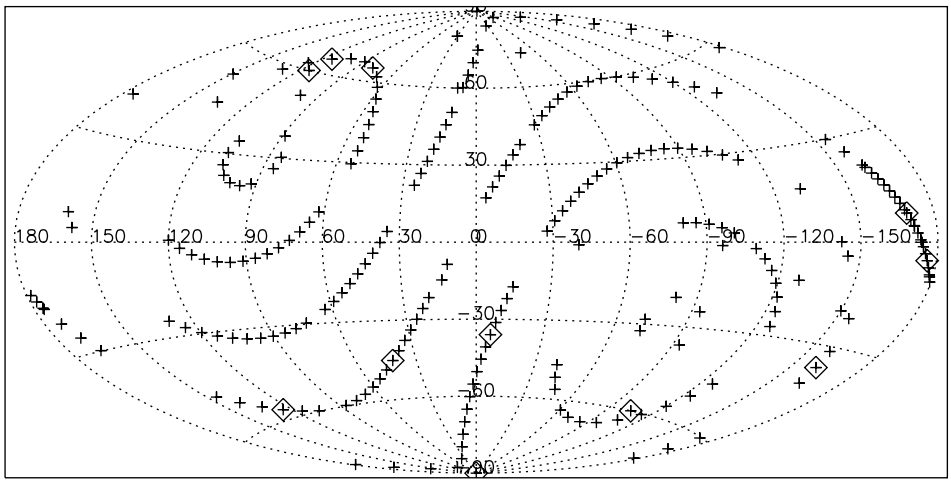

FIG. 1.—Galactic coordinates of *CHIPS* boresight for the fields analyzed in this work. Large diamonds indicate targets where the brightest EUV flux was observed by *CHIPS*. The long axis of the *CHIPS* field of view spans 25° and is generally parallel to lines of ecliptic longitude and perpendicular to the strings of boresight symbols; thus, the sky coverage has minimal gaps when targets are adjacent.

to monthly charged-particle flat fields. We measured pixel-to-pixel excursions relative, not to a smooth polynomial, but to a scaled background formed by summing the charged particles from the remaining months. This analysis, like the analysis applied to the flight photon spectra, includes a type of flat-field correction. We found a distribution of excursions closely approximating a Poisson distribution, with no excess variance over shot noise. The monthly charged-particle flat fields contain a total number of counts corresponding to integration times of about 800,000 s at count rates characteristic of our normal observing conditions. Thus, our analysis technique allows us to reach the shot noise limit for ordinary spectra with integration times at least as deep as 800,000 s. We treat the shot noise in an 800,000 s integration as a limiting uncertainty for deeper observations, not because of evidence that systematic effects become significant at longer times, but because we have not yet shown their absence.

The wavelength scale is based on preflight measurements, offset by a (constant) ~1 Å determined from the bright He II 256.3 Å feature, which is present in essentially all the observations. Temporal variations in the measured centroid of the He II feature show a dispersion of about 0.2 Å. Periodic observations of the moon, which provide a weakly reflected solar spectrum that includes the features of Fe IX–XII, confirm that the adopted wavelength scale provides a good fit near the center of the spectral band, and that the relative throughput of the filter panels is as measured preflight. The measured fluxes of both the He II feature and the lunar spectrum are in good agreement with preflight expectations, suggesting that the instrument throughput has not declined since laboratory calibration. Additional details of the on-orbit verification will be presented in a subsequent work.

3. OBSERVATIONAL RESULTS

Over most of the *CHIPS* spectral band, and certainly near the wavelengths of the iron lines, photoelectric absorption from the neutral interstellar medium limits the observable path length to at most a few hundred parsecs. Thus the only astrophysical source we expect to see is emission from the local hot bubble that should be isotropic (within a factor of a few) on the sky.

In Figure 2, we show a spectrum from 150 to 200 Å, binned at 0.5 Å. This is the complete spectrum for the CY 2003–2004 narrow-slit program, representing 13.2 Ms of effective observing time, inclusive of all latencies or "dead times." About 74% of the data were collected during orbital day, 26% during orbital night. Both filter panels are included in the histogram. Much of the observing time was directed at regions where the EUV brightness was expected to be high, based on high soft X-ray brightness, low column density of neutral hydrogen, etc. In Figure 2, we also show a scaled, charged-particle background spectrum and an APEC/CHIANTI model (discussed below) with parameters from one model for the local hot bubble (emission measure 0.0038 cm^{-6} pc, $\log T = 6.1$, foreground absorption 2×10^{18} cm^{-2}) folded through the instrument response. At most wavelengths, the small-scale variations in the spectrum are closely tracked by the charged-particle background, but there is a modest excess of counts coincident with the expected position of the Fe IX line at 171.1 Å. For reference, the estimated strength of the observed line is about 6 LU. The model prediction exceeds the measured flux in this line by only a factor of a few. However, essentially all of the other model lines arise from higher ionization

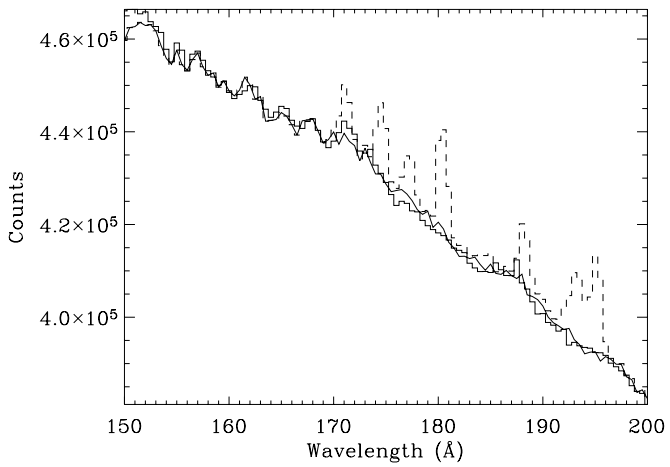

FIG. 2.—Co-added spectrum from 150 to 200 Å of all fields, summing both filter panels (*solid histogram*). Vertical axis shows total counts in bins of 0.5 Å. We also show a scaled, charged-particle background spectrum (*solid line*) and background plus predictions of a "canonical" local hot bubble model with temperature of $10^{6.1}$ K and an emission measure of 0.0038 cm^{-6} pc (*dashed histogram*), adapted to the same spectral bin size. The most significant excess observed above background is near 171 Å.

TABLE 1
EUV Line Flux Limits

Observed Wavelength (Å)	Filter	Flux[a] (LU)	Statistical Uncertainty[c]	Bright Flux[b] (LU)	Statistical Uncertainty[c]	Limiting Uncertainty[d]	Potential Feature[e]
116.7	Poly + Zr	0.2	0.9	−0.36	1.8	2.3	Ne VII 116.7
122.6	Poly + Zr	−0.4	0.9	−2.5	1.7	2.2	Ne VI 122.5, 122.7
168.2	Zr	3.4	2.3	−1.2	4.6	5.7	Fe VIII 167.5, 168.2, 168.6, 169.0
171.1	Large Al + Zr	6.2	1.5	20.0	2.9	3.6	Fe IX 171.1
174.5	Large Al + Zr	2.5	1.6	−2.3	3.1	3.8	Fe X 174.5
177.2	Large Al + Zr	−5.4	1.7	−5.6	3.3	4.0	Fe X 177.2
180.4	Large Al + Zr	−3.5	1.8	0.1	3.5	4.4	Fe XI 180.4
185.8	Large Al	2.8	2.1	0.9	4.1	5.0	Fe VII 185.2, 186.6
188.3	Large Al	−4.0	2.2	0.9	4.3	5.3	Fe XI 188.3
194.5	Large Al	−1.9	2.3	0.2	4.4	5.6	Fe XII 193.5, 195.1
202.0	Large Al	−0.4	2.6	1.2	4.9	6.1	Fe XIII 202.0
224.7	Large Al + Small Al	1.1	2.7	5.9	5.1	6.7	S IX 224.7

Note.—Data generally correspond to two filter panels co-added. Where the S/N was higher for a single panel alone, only that panel was used. At 185.8 Å, only the large aluminum filter was used, because of a transient "hot spot" on the detector in a region under the zirconium panel. Uncertainties are 1 σ.

[a] Determined from integrated spectrum of the full 13.2 Ms of observational data.

[b] Determined from spectrum formed of the 1.3 Ms when the 171.1 Å feature is brightest.

[c] Uncertainty arising from shot noise in the spectrum and background subtraction process for the preceding column; systematic effects are not included.

[d] Shot noise for an 800,000 s observation, adopted in the quantitative analysis of the spectra.

[e] Contains the brightest line(s) expected from plasma between about $10^{5.6}$ and $10^{6.2}$ K; at cooler temperatures, additional features discussed in the text begin to contribute.

stages of iron, with predicted fluxes that greatly exceed the limits set by the observations.

Individual observations can be identified in which the EUV emission is brighter than in the integrated spectrum. For this analysis, we consider all observations with duration greater than 20 ks. Of the 166 such observations, there are 11 in which the 171.1 Å feature is detected to a S/N (based on shot noise) greater than 2, and for which the measured flux exceeds 10 LU. Based on Gaussian statistics, only ~4 observations should have exceeded a 2 σ threshold if the true line flux were zero. The fact that 11 do indicates that for most of these observations, the detection is not a statistical artifact. Furthermore, examination of the two-dimensional detector images shows that the observed line is extended along the full slit length, ruling out a detector hot spot. Thus, despite the relatively low amplitude of the feature even when it is bright, we are confident that it represents real photons entering the instrument through the narrow entrance slits. As can be seen on Figure 1, the bright fields are generally found at high latitudes, and there is a tantalizing grouping near $b = 60^\circ$, $l = 100^\circ$. However, the most striking feature of the bright observations is that only one of the 11 occurred at night, and that observation was of relatively low observing time (about 50 ks). The overwhelming majority of the bright observing time (96%) corresponds to daytime data. This greatly exceeds the daytime fraction for the observations generally, and suggests that much of the emission is not interstellar in origin but has a more local origin. The flux of the 171.1 Å line in the combined spectrum of all the bright targets is 20 LU, with a 1 σ uncertainty (shot noise) of about 3 LU.

Depending on the detailed gas temperature and elemental abundances, a variety of features might potentially be detected in the *CHIPS* spectra. In Table 1, we show the flux at a variety of wavelengths corresponding to bright single features or line clusters. Results from both the complete data set and the EUV bright observations are presented. To set the limits shown in Table 1, we compare the spectrum to the scaled background over a wavelength interval 1.4 times the FWHM resolution element at each stated wavelength. This interval is broad enough to capture essentially all of the flux of a line at the stated wavelength, and allows us to neglect the 0.2 Å uncertainty in the wavelength scale. We also show the error in the mean flux (based on shot noise). This shot noise error is small because the combined integration time for all targets is 13,200,000 s. As discussed above, we have verified independently that systematic effects can be neglected for integration times of up to about 800,000 s, but not necessarily for 13,200,000 s. Therefore, in the analysis below, we take as the 1 σ uncertainty in each line flux a value corresponding to the shot noise limit for an ~800,000 s integration and show this uncertainty in Table 1.

The faintness of the EUV emission makes characterizing its origin difficult. Before launch, we expected, or at least hoped, that *CHIPS* would record signals of ~50 LU or more. Such signals could be detected to 3 σ significance in observing times of ~200 ks. The first year's data set would provide nearly 70 independent spectra at this sensitivity level, facilitating study of how the EUV brightness might vary with astrophysical parameters or with orbital conditions (day/night cycle, zenith angle, Sun avoidance, etc.). In the actual data, the typical fluxes are an order of magnitude fainter, demanding integrations roughly 100 times deeper to achieve a given S/N. The narrow-slit data set important limits on the brightness of EUV emission lines and indicate that the periods when EUV emission is detected are probably contaminated by a foreground source associated with orbital daytime. However, the narrow-slit data provide too few independent measurements at sufficient sensitivity to allow the spatial/temporal/other variability of the emission to be explored in detail. Accordingly, the instrument was switched to wide-slit observing mode in early 2004.

4. CIE PLASMA MODELING

In this section, we analyze the complete integrated spectrum, without excluding the EUV bright observations or otherwise correcting for the daytime foreground emission. This is because the detailed foreground contribution is difficult to quantify, and because, at the 95% confidence level, the constraints on plasma emission measure are dominated by the limiting uncertainties rather than the best-fit EUV line fluxes. If the positive best-fit flux(es) in the integrated spectrum were shown to arise entirely

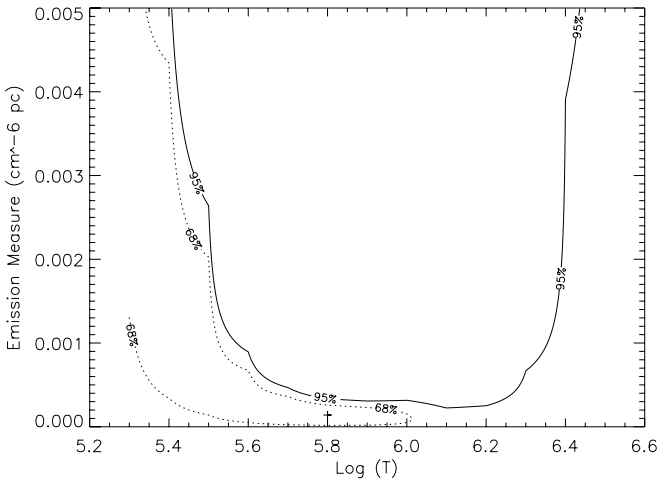

FIG. 3.—Constraints on temperature and emission measure based on *CHIPS* observations, and APEC/CHIANTI equilibrium ionization plasma code with solar abundances. See text for discussion.

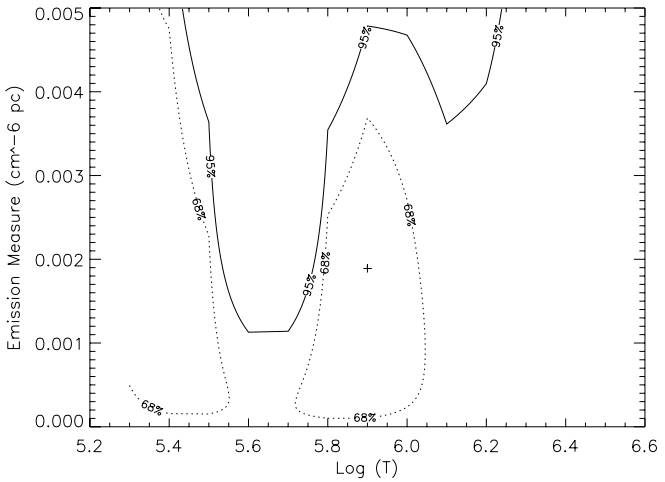

FIG. 4.—Constraints on temperature and emission measure based on *CHIPS* observations, and APEC/CHIANTI equilibrium ionization plasma code with depleted "warm cloud" abundances. See text for discussion.

from the foreground, the constraints on plasma emission measure would fall by at most a factor of 1.8 compared to those presented below.

To interpret the *CHIPS* data, we apply the predictions of the APEC plasma code, utilizing a grid of line emissivities at temperature steps of 0.1 dex.[1] We also include features of Fe VIII from the CHIANTI line list (version 4.2; Young et al. 2003), as these features are not present in the current release of APEC. Emissivities are calculated in the low-density limit.

We generate a grid of model spectra with steps of 0.1 in the logarithm of the temperature and 0.00001 in the emission measure. For each of the wavelengths at which we have a flux limit in Table 1, we sum the fluxes of the nearby modeled spectral lines, weighting each by the appropriate value of the resolution kernel. We apply a foreground interstellar absorption with a column of 2×10^{18} cm^{-2}, compare the summed model line flux(es) with the observational limits set by the integrated spectrum presented in Table 1, calculate a value for χ^2, and set confidence intervals for two free parameters following Lampton et al. (1976).

For gas with solar abundances, the *CHIPS* data constrain the plasma temperature and emission measure, as shown in Figure 3. The best-fit parameters correspond to a temperature around $10^{5.8}$ K and an emission measure of about 0.00014 cm^{-6} pc. The 68% and 95% confidence contours are illustrated in Figure 3. The central result is that, subject to the model assumptions, the *CHIPS* data constrain the emission measure tightly for temperatures between about $10^{5.55}$ and $10^{6.4}$ K. At $10^{6.0}$ K, the 95% upper limit is about 0.0004 cm^{-6} pc.

For depletions in which the gas-phase iron abundance is reduced by a factor of only a few compared to solar, depletion trades off directly with the allowed emission measure. This is because the modeled iron features are significantly brighter than all other features in the *CHIPS* band unless iron is depleted significantly. The iron abundance inferred from an X-ray spectrum of local hot gas was about 30% of solar (Sanders et al. 2001); for such gas, the constraints on emission measure contained in Figure 3 should simply be scaled upward by a factor of about 3.

To explore the case of highly depleted gas, we have repeated the analysis described above assuming "warm cloud" depletions from Savage & Sembach (1996). In this model, iron is depleted by 1.2 dex, or to a value about 1/16 of solar, and other elements are depleted as well. We show the corresponding constraints on plasma temperature and emission measure in Figure 4.

To explore the degree to which our results are dependent on the iron lines, we constructed an artificial set of depletions in which the gas-phase iron abundance is zero, and all other elements have solar abundances. For that model, the constraints on emission measure are similar to those shown in Figure 4. Thus, the warm cloud depletions treated above already suppresses the iron sufficiently that the emission measure is limited by nondetection of lines of other elements of relatively low depletion (for example, a cluster of O V and O VI lines near 171–173 Å).

5. DISCUSSION

The *CHIPS* data show that the EUV iron lines are extremely faint. The fluxes analyzed here are likely to include a local/foreground component, leaving even less room for interstellar flux. Although previous works have suggested that the Fe features are weaker than predicted by collisional ionization equilibrium models, some of those results have rested on uncertain and untestable assumptions. Using a point-source spectrometer aboard the *Extreme Ultraviolet Explorer* (*EUVE*), Jelinsky et al. (1995) set an upper limit to the emission measure near $10^{5.8}$ K, which is also lower than expected for the local hot bubble (but not as tight as our limits). However, owing in part to the low resolution of the instrument, it was difficult to confirm that the very large background in the *EUVE* signal could be subtracted precisely. Bloch et al. (2002) interpret *ALEXIS* multilayer imaging of the diffuse background with a model in which an astrophysical EUV flux is assumed to scale with the Wisconsin *B*-band map, and conclude that the Fe emission is no more than about 1/10 of the predicted flux level. The pulse-height distribution for the Be-band proportional counter Wisconsin rocket data has been reported to require significant depletions (i.e., the pulse height distribution is inconsistent with full-strength iron lines: Bloch 1988). Using a rocket-borne calorimeter, McCammon et al. (2002) report a detection of emission from Fe IX, X, and XI (unresolved) with a combined flux of about 100 LU, significantly greater than allowed by the *CHIPS* data. The calorimeter signal (4 events) exceeds the expected background (0.3 events) and sets a 90% lower limit of about 40 LU on the combined line strengths, a limit well above the best-fit *CHIPS* results. Whether the difference in results arises from instrument calibration effects, a statistical oddity, or genuine differences in fields observed (due to

[1] APEC EUV line emissivities provided by N. Brickhouse.

astrophysical or local effects) is not yet clear. In any case, the *CHIPS* observations set robust constraints on important individual spectral lines.

The *CHIPS* results are at variance with X-ray measurements interpreted with similar models and subject to the same assumptions (solar abundances, collisional ionization equilibrium). As noted above, temperatures greater than $10^{6.0}$ K, and emission measures an order of magnitude higher than the 95% upper limits of Figure 3, have been reported. Depletion of iron relative to other heavy elements generally helps reconcile the EUV and X-ray results, but the depletions reported previously have been only moderate: roughly a factor of 3 reduction in the gas-phase abundance of elements including iron (Sanders et al. 2001). However, it must be noted that the abundances of Sanders et al. (2001) were best-fit values only, and thus the possibility remains that much lower abundances might be consistent with their observational data. The *CHIPS* results are qualitatively consistent with a poster presented by Bellm (2003), concluding that a combination of depletion and a lower temperature ($10^{5.85}$ K) in the local hot gas provides a better fit to the broadband X-ray colors than undepleted, hotter models; see also Bellm & Vaillancourt (2005).

Foreground absorption alone cannot reconcile the *CHIPS* and X-ray results. A foreground column density of N(H I) of 1.5×10^{19} cm^{-2} is required in order for the hydrogen and associated helium to attenuate the iron features by about a factor of 10. Such a foreground column would violate the observed constancy of the *B*-band–Be-band ratio (Juda 1988).

We have not obtained a detailed charge-exchange spectrum that can be compared directly with the *CHIPS* data. We note, however, that the solar wind (especially the slow equatorial wind) is enriched in Fe as a result of the well-known "FIP" effect, and that the dominant ionization stages are Fe X and Fe XI (Schwadron et al. 1999; von Steiger 1994). Charge exchange provides at least a plausible origin for the Fe IX emission detected in the bright observations. The greater its contribution to the observed EUV flux, of course, the tighter the constraints on emission attributable to an interstellar plasma.

Reconciling in detail the *CHIPS* observations with the existing body of X-ray data on the local bubble will evidently require careful treatment of depletion effects. Whether the models must also include multitemperature structures or nonequilibrium interstellar conditions in the local bubble is not yet known.

CHIPS is supported by NASA grant NAG 5-5213. We are grateful to the *CHIPS* hardware and flight operations teams, David Pierce, Randy Kimble, and the many review panel members whose participation strengthened the project. Nancy Brickhouse graciously provided the APEC EUV line emissivities in a convenient format and, with Randall Smith, patiently answered questions as to format and content. We used the data compiled by CHIANTI, a collaborative project involving the NRL (USA), RAL (UK), and the Universities of Florence (Italy) and Cambridge (UK).

REFERENCES

Bellm, E. C. 2003, BAAS, 203, 11104
Bellm, E. C., & Vaillancourt, J. 2005, ApJ, in press
Bloch, J. J. 1988, Ph.D. thesis, Univ. Wisconsin, Madison
Bloch, J. J., Roussel-Dupre, D., Theiler, J., & Johnson, E. 2002, in ASP Conf. Ser. 264, Continuing the Challenge of EUV Astronomy: Current Analysis and Prospects for the Future, ed. S. Howell et al. (San Francisco: ASP), 243
Breitschwerdt, D., & Schmutzler, T. 1994, Nature, 371, 774
Cravens, T. E., Robertson, I. P., & Snowden, S. L. 2001, J. Geophys. Res., 106, 24883
Crawford, I. A., Lallement, R., Price, R. J., Sfeir, D. M., Wakker, P. P., & Welsh, B. Y. 2002, MNRAS, 337, 720
Freyberg, M. J. 1998, in IAU Colloq. 166, The Local Bubble and Beyond, ed. D. Breitschwerdt, M. J. Freyberg, & J. Truemper (New York: Springer), 113
Hurwitz, M., et al. 2003, Proc. SPIE, 5164, 24
Janicik, J., et al. 2003, Proc. SPIE, 5164, 31
Jelinsky, P. J., Vallerga, J. V., & Edelstein, J. 1995, ApJ, 442, 653
Jenkins, E. B., et al. 2000, ApJ, 538, L81
Juda, M. 1988, Ph.D. thesis, Univ. Wisconsin, Madison
Kimble, R. A., et al. 1993, ApJ, 404, 663
Kuntz, K. D., & Snowden, S. L. 2000, ApJ, 543, 195
Lallement, R., et al. 2004, A&A, 418, 143
Lampton, M., Margon, B., & Bowyer, S. 1976, ApJ, 208, 177
Marckwordt, M., et al. 2003, Proc. SPIE, 5164, 43
McCammon, D., & Sanders, W. T. 1990, ARA&A, 28, 657
McCammon, D., et al. 2002, ApJ, 576, 188
Sanders, W. T., et al. 2001, ApJ, 554, 694
Savage, B. D., & Sembach, K. R. 1996, ARA&A, 34, 279
Schwadron, N. A., Fisk, L. A., & Zurbuchen, T. H. 1999, ApJ, 521, 859
Sfeir, D. M., Lallement, R., Crifo, F., & Welsh, B. Y. 1999, A&A, 346, 785
Sholl, M., et al. 2003, Proc. SPIE, 5164, 63
Sirk, M. M., et al. 2003, Proc. SPIE, 5164, 54
Snowden, S. L., Egger, R., Finkbeiner, D. P., Freyberg, J. J., & Plucinsky, P. P. 1998, ApJ, 493, 715
Vallerga, J. V., & Welsh, B. Y. 1995, ApJ, 444, 702
von Steiger, R. 1994, Ph.D. thesis, Univ. Bern
Young, P. R., et al. 2003, ApJS, 144, 135